# Reports

## Lunar Shape via the Apollo Laser Altimeter

Abstract. *Data from the Apollo 15 and Apollo 16 laser altimeters reveal the first accurate elevation differences between distant features on both sides of the moon. The large far-side depression observed in the Apollo 15 data is not present in the Apollo 16 data. When the laser results are compared with elevations on maps from the Aeronautical Chart and Information Center, differences of 2 kilometers over a few hundred kilometers are detected in the Mare Nubium and Mare Tranquillitatis regions. The Apollo 16 data alone would put a 2-kilometer bulge toward the earth; however, the combined data are best fit by a sphere of radius 1737.7 kilometers. The offset of the center of gravity from the optical center is about 2 kilometers toward the earth and 1 kilometer eastward. The polar direction parameters are not well determined.*

The laser altimeter data obtained from the Apollo 15 and Apollo 16 missions provide two elevation cross sections of the moon separated by 35° of latitude. These data are the first set obtained by a highly accurate method of measuring lunar topography over global distances. Before this, Earth-based photography was used; shadows were measured and stereoscopic effects were accounted for to determine surface elevations. However, the errors were large over distances of hundreds of kilometers, and the results were extremely poor near the limbs (*1, 2*). There are also many independent measurements of lunar elevations, such as the elevations of the Ranger impact points (*3*), the Surveyor landing sites (*4*), the Apollo survey sites (*5*), and the Saturn booster impact points (*5*), as well as elevations determined from the velocity-height data of the Lunar Orbiter (*6*) and from Earth-based radar (*7*), landmark tracking (*8, 9*), and laser ranging retroreflectors (*10*). All of these results are from front-side observations at random points, except for ten far-side landmark points obtained with the Apollo sextant.

With complete 360° profiles, analysis can proceed with the examination of the best figure parameters and the verification of other results. Although another set of laser data is expected from Apollo 17, its coverage will be similar to that of Apollo 15 and will not significantly enhance these basic results.

The data consist of measurements of the distance from the orbiting Command and Service Module (CSM) to the lunar surface at intervals of approximately 20 seconds (that is, approximately every 30 km along the surface track). The altimeter has a surface spot size of 30 m and an accuracy of 2 m. There are slight corrections for timing and attitude position which can be applied to the data for ultimate resolution; however, these corrections were not applied because they amount to only a few meters and do not affect the results. The amount of data used for this analysis is shown in Table 1, and the location of the cross sections is shown in Fig. 1.

To extract the lunar shape parameters from the data, the position of the CSM must be known. This was accomplished by reducing the data from Earth-based radio tracking of the CSM. Essentially, these are line-of-sight speed measurements taken every 10 seconds. These observations, made simultaneously from several tracking stations on the earth, were processed by a large computer program having a theoretical model of the earth-moon system. A least-squares regression was performed, and a unique orbit for the CSM was determined. The accuracy of this orbit is the governing accuracy of our results. The primary uncertainty in the orbit does not come, however, from the quality of the tracking data, but from the description of the lunar gravity field. The L1 model (*11*) used in this reduction does not account for high-frequency position variations caused by such things as mascons. It is estimated that an upper bound on the uncertainty in the orbit is 400 m in the direction of the laser measurement. More realistic gravity models could be employed, but they would only represent the front-side field, and all laser measurements on the back would again be corrupted. Until good far-side gravity measurements are obtained (which is not foreseeable in the near future), this position uncertainty will remain near the 100-m level. However, this error is of the bias type and remains relatively constant over a 1000-km portion of the orbit.

Once the CSM orbit was established, the remaining steps were straightforward. The laser altimeter readings were subtracted from the corresponding selenocentric radius vectors of the CSM orbit, and a complete lunar topographic profile was obtained. This profile is referred to the center of gravity of the moon rather than the optical figure, for the orbit determined from Doppler data is a dynamical solution about the center of gravity. The results of this differencing are shown in Fig. 2. Note the good agreement for the Smythii floor (*12*). It is fortunate that the two trajectories cross here in a relatively flat region, for on the opposite side (+180° of longitude) the highlands offer only a general trend. The large far-side depression [possibly correlated with the Russian feature (*13*)] observed on Apollo 15 is not evident in the Apollo 16 data. Oceanus Procellarum is more than 1 km lower in the southern hemisphere. The central highlands are a high region. The profiles of the large front-side basins with their flat floors are also evident. The large far-side basin of Hertzsprung can be seen in the Apollo 16 profile.

Not so evident are the deviations from the elevations on existing lunar maps. If one compares the elevations in Ptolemaeus with those in Mare

Table 1. Data used in the analysis for the lunar shape parameters. *N*, number of observations.

| Mission | Orbit number | *N* | Remarks |
|---|---|---|---|
| Apollo 15 | 15, 16 | 319 | Laser, complete orbit |
| Apollo 16 | 17, 18 | 279 | Laser, complete orbit |
| Apollos 8 to 16 | | 30 | Landmarks, sextant readings |
| Rangers 6 to 9 | | 4 | Time of impact |
| Surveyors 1 and 6 | | 2 | Landers, surface Doppler data |
| Lunar Orbiter I | | 73 | Velocity-height sensor for photography |

Nubium, the laser results are just about the opposite of those on lunar chart LAC 77 from the Aeronautical Chart and Information Center (ACIC) (*2*). Ptolemaeus is 1 km higher than Nubium, not lower as existing charts indicate. The same is true in the Tranquillitatis region. Since redundancy was obtained in the measurements made in this region during four other laser altimeter orbits in Apollo 16, the confidence level is extremely high. There will certainly be major revisions to lunar charts when the altimetry and photography data from the Apollo missions are thoroughly integrated, a job that ACIC and the U.S. Army Topographic Command are presently performing.

To obtain the shape parameters relative to the optical center, further least-squares regressions were performed by using offset sphere and offset ellipsoid models. (The regressions did not include data in the overlapping laser profile.) Listed in Table 2 are the solutions for various assumptions. It appears that the moon is nearly spherical with a radius of 1737.7 km, only 0.3 km from the presently accepted value of 1738.0. Slightly different results occur for each mission, but this is expected since Apollo 15 passed over the large ringed basins of Imbrium, Serenitatis, Crisium, and Smythii, and a large far-side depression. The results shown on line 6 in Table 2 (*14, 15*) make $Y$ the largest axis, which is contrary to presently accepted estimates. However, Apollo 16 passes over "more typical" terrain and restores the major axis along the earth-moon line (line 7). In fact, if one uses Apollo 16 data and tries to match Baldwin's (*1*) and Runcorn and Shrubsall's (*16*) examples of the maria and highland front-side elevations to determine a bulge toward the earth, the results on lines 8 and 9 occur. It appears to support the results of these authors. Also shown in Table 2 (lines 10 to 12) are results from other independent measurements, which yield similar estimates and attest to their validity.

The most striking result is the consistency of the center of gravity offset in both the $X$ and $Y$ directions. The lunar center of gravity is some 2 km closer to the earth than the optical center and is displaced 1 km eastward. [In Table 2 it can be seen that the estimates

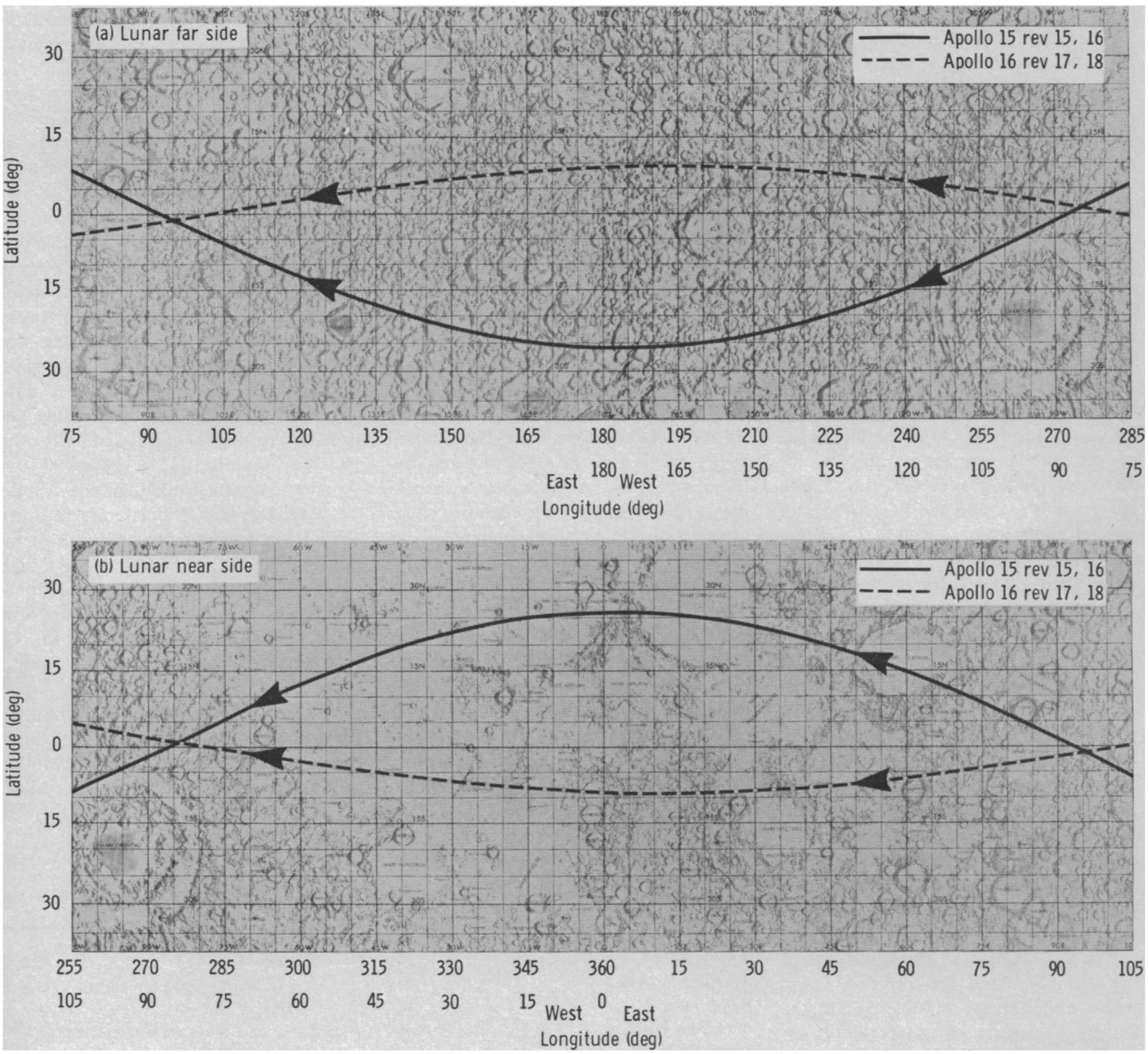

Fig. 1. Altimeter measurement traces.

of the $X$ and $Y$ axes and offsets are independent of the values used for $Z$ and $\Delta Z$ (lines 10 and 14).] This earthward offset was first noted in the analysis of the Ranger data (*3*) and has continually been a result of other experiments (*5–10*). There is certainly no doubt at all now with the two complete laser profiles. Solutions in the polar ($Z$) direction (lines 13 to 15) are shown for completeness; however, the authors do not believe these results, and wish to emphasize the need for observations in the polar regions.

The explanation for the center of gravity offset cannot be obtained with the presently known mascons for they are more than an order of magnitude too small. One might speculate on very large negative mass anomalies on the far side, which is not too unreasonable since the data from Apollo 15 and the Russian Zond 6 (*13*) do show large depressions. Another possibility is an

Table 2. Estimates of the lunar shape parameters. The $X$ axis is toward the earth, the $Y$ axis is east in the equatorial plane, and the $Z$ axis is the north polar axis. The offsets in these coordinates from the center of gravity to the optical center of the moon are $\Delta X$, $\Delta Y$, and $\Delta Z$. The abbreviations used are RA, Ranger impacts; SU, Surveyor landers; LMK, landmarks; $V/H$, velocity-height data from Lunar Orbiter I. "Lasers 15 and 16" refers to the Apollo 15 and Apollo 16 lasers. The weighting factors for the regression were: Laser, 1.0; RA, 5.2; SU, 5.2; LMK, 5.2; $V/H$, 2.9.

| Line | Shape | Data | X (km) | Y (km) | Z (km) | ΔX (km) | ΔY (km) | ΔZ (km) | Remarks |
|---|---|---|---|---|---|---|---|---|---|
| 1 | Sphere | Lasers 15 and 16 | 1737.7 | | | −2.20 | −1.10 | −1.0* | |
| 2 | Sphere | RA, SU, LMK, lasers 15 and 16 | 1737.8 | | | −2.05 | −0.91 | −1.0* | |
| 3 | Ellipsoid | Lasers 15 and 16 | 1737.8 | 1737.5 | 1738.0* | −2.07 | −1.11 | −1.0* | |
| 4 | Circle | Apollo 15 laser | 1737.1 | | | −1.76 | −1.19 | | (*9, 10*) |
| 5 | Circle | Apollo 16 laser | 1737.8 | | | −2.78 | −1.00 | | |
| 6 | Ellipse | Apollo 15 laser | 1736.4 | 1737.7 | | −1.79 | −1.15 | | (*9, 10*) |
| 7 | Ellipse | Apollo 16 laser | 1738.7 | 1736.7 | | −2.52 | −1.03 | | |
| 8 | Ellipse | Apollo 16 laser, front-side maria | 1737.6 | 1735.5 | | −2.1* | −1.2* | | 38 points, −60° to +60° longitude |
| 9 | Ellipse | Apollo 16 laser, front-side highland | 1741.1 | 1737.1 | | −2.1* | −1.2* | | 26 points, −110° to +110° longitude |
| 10 | Ellipsoid | RA, SU, $V/H$, LMK, lasers 15 and 16 | 1738.2 | 1737.4 | 1738.0* | −1.98 | −0.75 | −1.0* | |
| 11 | Ellipsoid | RA, SU, LMK, lasers 15 and 16 | 1738.0 | 1737.6 | 1738.0* | −2.07 | −0.91 | −1.0* | |
| 12 | Ellipsoid | RA, SU, LMK, $V/H$ | 1738.8 | 1736.8 | 1738.0* | −2.22 | +0.24 | −1.0* | |
| 13 | Ellipsoid | Lasers 15 and 16 | 1738.8 | 1737.6 | 1728.0 | −2.17 | −1.14 | +0.21 | Unconstrained $Z$ |
| 14 | Ellipsoid | RA, SU, $V/H$, LMK, lasers 15 and 16 | 1738.6 | 1737.5 | 1730.8 | −2.15 | −0.77 | −0.27 | Unconstrained $Z$ |
| 15 | Ellipsoid | RA, SU, $V/H$, LMK | 1738.8 | 1737.6 | 1733.9 | −2.14 | +0.30 | −2.58 | Unconstrained $Z$ |

* Not estimated but held at fixed value shown.

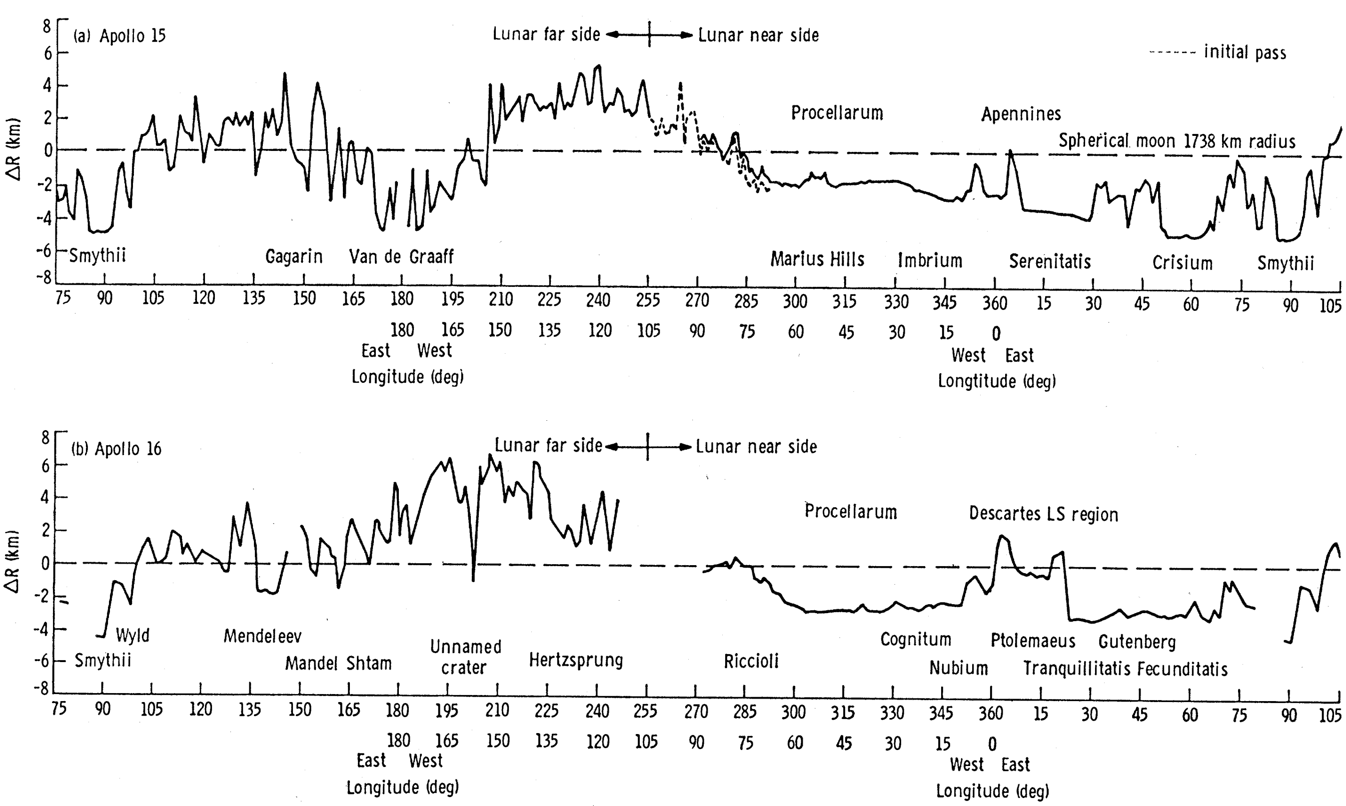


Fig. 2. Altitude profile or radius deviations from a 1738.0-km spherical moon.

offset core (*17*) or a difference in crustal thickness between the near side and the far side (*15*).

W. L. SJOGREN
*Jet Propulsion Laboratory, California Institute of Technology, Pasadena 91109*
W. R. WOLLENHAUPT
*NASA Manned Spacecraft Center, Houston, Texas 77058*

### References and Notes

1. R. Baldwin, *The Measure of the Moon* (Univ. of Chicago Press, Chicago, 1963).
2. Lunar Charts LAC 1 through LAC 144, Aeronautical Chart and Information Center, St. Louis, Mo.
3. W. L. Sjogren, in *Measure of the Moon*, Z. Kopal and C. L. Goudas, Eds. (Reidel, Dordrecht, Netherlands, 1967), pp. 341–343.
4. F. B. Winn, *Surveyor Project Final Report* (Technical Report 32-1265, Jet Propulsion Laboratory, Pasadena, Calif., 1968), part 2, pp. 407–438.
5. W. R. Wollenhaupt and G. A. Ransford, *Bull. Amer. Astron. Soc.* **3**, 272 (1971).
6. H. R. Compton and W. R. Wells, *Determination of Lunar Equatorial Radius Using Image-Motion Compensation Sensor Data from Lunar Orbiter I* (NASA TN D-5231, National Aeronautics and Space Administration, Washington, D.C., 1969).
7. A. Shapiro, E. A. Uliana, B. S. Yaplee, S. H. Knowles, in *Moon and Planets*, A. Dollfus, Ed. (North-Holland, Amsterdam, 1968), vol. 2, pp. 34–46.
8. W. R. Wollenhaupt, R. K. Osborn, G. A. Ransford, *Moon* **5** (Nos. 1/2), 149 (1972).
9. W. H. Michael, Jr., in *The Figure of the Moon* (NASA SP 201, National Aeronautics and Space Administration, Washington, D.C., 1969), pp. 63–64.
10. J. E. Faller *et al.*, in *Apollo 15 Preliminary Science Report* (NASA SP 289, National Aeronautics and Space Administration, Washington, D.C., 1971), pp. 14-1 to 14-6.
11. The L1 lunar gravity model is described by $GM_{☾} = 4902.78$ km$^3$/sec$^2$ and the spherical harmonic coefficients $J_{20} = 2.07108 \times 10^{-4}$, $J_{30} = -0.21 \times 10^{-4}$, $C_{22} = 0.20716 \times 10^{-4}$, $C_{31} = 0.34 \times 10^{-4}$, and $C_{33} = 0.02583 \times 10^{-4}$.
12. The laser altimeter radius values agree very well with those obtained by Watts from limb outline measurements on photographic plates from the U.S. Naval Observatory (*1*).
13. B. N. Rodionov *et al.*, *Kosm. Issled.* **9**, 450 (1971).
14. W. R. Wollenhaupt and W. L. Sjogren, *Moon* **4** (Nos. 3/4), 337 (1972).
15. W. M. Kaula, G. Schubert, R. E. Lingenfelter, W. L. Sjogren, W. R. Wollenhaupt, in *Proceedings of the 3rd Lunar Science Conference* (M.I.T. Press, Cambridge, Mass., 1972), vol. 3, p. 2189.
16. S. K. Runcorn and M. H. Shrubsall, *Phys. Earth Planet. Interiors* **1**, 317 (1968).
17. G. A. Ransford and W. L. Sjogren, *Nature* **238**, 260 (1972).
18. Supported by NASA contract NAS 7-100.

6 October 1972

## Source Parameters for Stick-Slip and for Earthquakes

Abstract. *Source parameters of stick-slip friction events measured in the laboratory show particle and rupture propagation velocities which are similar to those observed for earthquakes and inferred from seismic source theory. This dynamic similarity strongly supports the idea that stick-slip is the mechanism for shallow earthquakes.*

Brace and Byerlee (*1*) suggested stick-slip friction as a possible mechanism for shallow earthquakes because it produces jerky displacements and qualitatively explains, in terms of partial stress drops, the small stress release inferred for earthquakes compared with inherent rock strengths. We began a systematic laboratory study of the dynamic properties of stick-slip in order to understand more clearly the stick-slip mechanism and to suggest geophysical measurements that would indicate whether earthquake and stick-slip mechanisms are similar. Our results show that the dynamic behavior of stick-slip is nearly identical with that of earthquakes and provide a strong argument for the stick-slip model of shallow earthquakes.

These measurements were made with a new type of friction testing machine (*2*). The sample is a slab 10 by 18 by 3 cm, with a sliding surface formed by a ground cut made diagonally at 30° across its major face. The sample is placed in a biaxial load frame and loaded on two perpendicular edges with hydraulic rams, while the other edges are allowed to move freely on roller bearings in such a way as to allow unconstrained slip on the 30° "fault." Stresses are maintained uniform to within 10 percent along the entire fault and normal stresses up to about 1 kb are possible.

Particle velocity was measured directly across the fault by using either a differential capacitance displacement transducer or a linear variable resistor mounted directly on the specimen and across the central part of the fault. The velocities and general wave forms from the two different transducers agree well; thus, the transducer output faithfully reproduces the actual displacements. A typical curve of displacement as a function of time for a stick-slip event is shown in the lower right corner of Fig. 1. The displacement source time function is roughly a truncated ramp, with a gradual beginning and termination. The ramp systematically steepens with increasing stress drop (and hence total stress). The velocities were measured by fitting a straight line through the inclined section of the ramp by eye. The estimated errors in this procedure are about 10 percent.

Table 1. Rupture velocities, $V_r$, for stick-slip events at shear and normal stresses $\tau_1$ and $\sigma_1$. The shear stress drop is $\Delta\tau$.

| $V_r$ (km/sec) | $\sigma_1$ (bars) | $\tau_1$ (bars) | $\Delta\tau$ (bars) |
|---|---|---|---|
| 2.3 | 27 | 16 | 5 |
| 2.4 | 26 | 15 | 6 |
| 3.0 | 35 | 24 | 8 |
| 3.3 | 237 | 90 | 19 |
| 3.5 | 252 | 94 | 23 |
| 4.1 | 257 | 102 | 32 |
| 4.0 | 280 | 94 | 20 |
| 4.7 | 291 | 114 | 50 |
| 4.7 | 320 | 101 | 30 |
| 4.7 | 351 | 125 | 22 |
| 4.7 | 363 | 115 | 40 |
| 3.5 | 361 | 122 | 39 |
| 4.6 | 383 | 127 | 47 |
| 4.8 | 395 | 143 | 52 |
| 4.7 | 420 | 147 | 49 |

The rupture velocity was measured by photographing the output of four axial piezoelectric transducers (accelerometers) displayed on an oscilloscope. The transducers were spaced evenly at 3-cm intervals along one side of the fault and at 5 mm from the fault edge. The passage of the rupture front was visible as a large pulse with a relatively long period followed by a higher frequency coda. The propagation time between different transducers was measured by using the first sharp break in the signal and the velocities computed. The velocities obtained between different transducers agreed within the assigned experimental error of about ± 15 percent, which was largely based on difficulties in choosing the first break. Richards (*3*) suggests that a large acceleration may occur before the passage of the rupture front, thus making its identification difficult, but as long as the recorded acceleration pulse shapes are uniform along the fault the rupture velocity will be correctly measured. Changes in the acceleration pulse shape along the fault were occasionally observed, but rupture velocities were only measured from uniform signals. Our observations are that the rupture accelerates to its terminal velocity very rapidly, that is, within about 3 cm. This contrasts with a fracture in virgin rock, which takes 20 to 30 cm to reach its terminal velocity (*4*).

Figure 1 and Table 1 present laboratory measurements of particle velocity and rupture velocity as a function of stress and stress drop for stick-slip between ground (80-grit wheel) surfaces of Westerly granite. The particle velocities (one half the velocity of one side of the fault with respect to the other)